SCIENTIFIC REPORTS
nature research

OPEN

A Complete Formula of Ocean Surface Absolute Geostrophic Current

Peter C. Chu

Absolute geostrophic current at the ocean surface (*S*) contains three components: (1) absolute geostrophic current at the geoid undulation (*N*), (2) geostrophic shear (between *S* and *N*) due to horizontal gradient of dynamic ocean topography, and (3) geostrophic shear (between *S* and *N*) due to horizontal gradient of density. However, only the second component is used to represent the surface absolute geostrophic current in physical oceanography and satellite geodesy. Four public datasets are used to calculate each component. Evident difference between the surface absolute geostrophic current and the second component (i.e., geostrophic shear due to horizontal gradient of dynamic ocean topography) was found by the statistical characteristics with the relative root mean square difference of 0.605. It shows that the common practice in physical oceanography and satellite geodesy is not correct. The horizontal gradient of dynamic ocean topography alone cannot be claimed as the surface absolute geostrophic current.

Ocean surface absolute geostrophic current (AGC) is the linkage between oceanography and satellite geodesy through dynamic ocean topography D, which is the sea surface height (S) (waves and tides filtered out) relative to the geoid undulation (N), $D = S - N$. Before satellites coming into practice, the two disciplines (oceanography and geodesy) were almost no connection. The gravity measurements over the ocean were very sparse. The marine geoid undulation N would coincide with the average level of sea surface height if the ***water were at rest***. With such a theoretical hypothesis (no motion at N), it is a common practice in oceanography that the horizontal gradient of S relative to the level of no motion (to be considered as D) represents the AGC at S. At that time, the geodetic community did not use the surface AGC.

After satellites coming into practice, S is measured by satellite altimetry (relative to ellipsoid)[1,2]; N (also relative to ellipsoid) is determined by gravity models with satellite measurements, such as Gravity field and steady-state Ocean Circulation Explorer (GOCE)[3], Gravity Recovery and Climate Experiment (GRACE)[4], and combined GOCE-GRACE[5]. The mean dynamic ocean topography (MDOT) is obtained through subtracting N from mean S. The MDOT calculated from satellite measurements is different from the classical conception (no motion at N)[6].

Now, the two communities have common interest on MDOT through the surface AGC. The oceanographic community uses the satellite determined MDOT to get mean general ocean circulation, i.e., surface AGC. The geodetic community uses the surface AGC to verify the static gravity models. Questions arise: Is water at rest at the given N in the oceans? Does horizontal gradient of MDOT represent the mean surface AGC? To answer these questions, a complete formula of ocean surface AGC is presented on the base of geostrophic and hydrostatic balances. It contains three parts: (1) AGC at N, (2) geostrophic shear from N to S due to horizontal gradient of MDOT, and (3) geostrophic shear from N to S due to horizontal gradient of density. The general practice in oceanography and geodesy only uses the second part to represent the surface AGC.

When N is given, it is very easy for an oceanographer to identify if N is a level of no motion. In fact, satellite measurements, such as altimetry for S and gravimetry from GOCE and GRACE for N, determine MDOT with a minimum value of −1.9981 m and a maximum value of 1.9538 m (see website: https://grace.jpl.nasa.gov/data/get-data/dynamic-ocean-typography/). It is hard to imagine that a level (i.e., the marine geoid N) within 2 m above and below the ocean surface (S) would be a level of no motion. The AGC at N can be determined from temperature and salinity profiles using the existing inverse methods such as the β-spiral[7], box model[8], and P-vector[9–12]. The geostrophic shear between S and N due to density can be obtained from temperature and salinity

Naval Ocean Analysis and Prediction Laboratory, Department of Oceanography, Naval Postgraduate School, Monterey, USA. email: pcchu@nps.edu

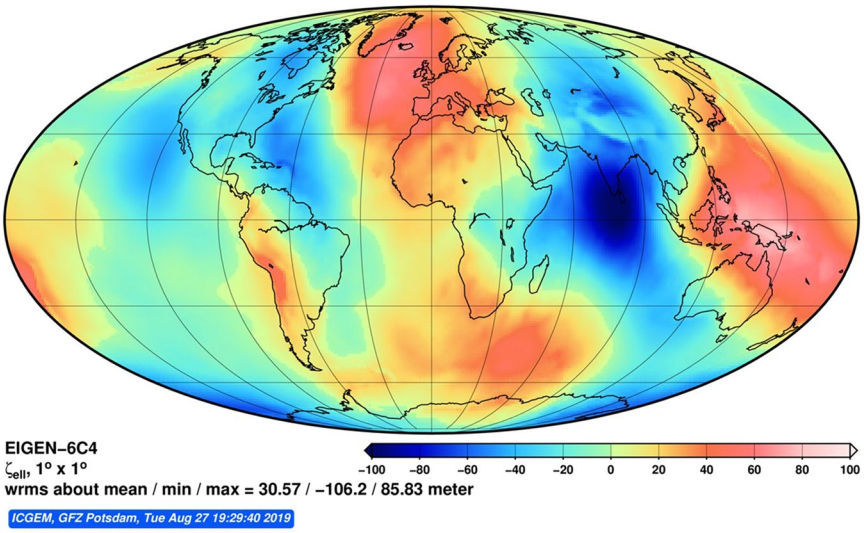

Figure 1. Digital data for EIGEN-6C4 geoid undulation (N) with 1° × 1°, computed online at the website http://icgem.gfz-potsdam.de/home.

profiles. Thus, the three parts of the surface AGC can be evaluated, and so as the errors of using horizontal gradient of MDOT only for the surface AGC.

A Complete Formula

The global oblate reference ellipsoid is used in geodesy with the semi-major axis (used for the Earth radius) as the equatorial reference and the semi-minor axis as the distance between the Earth center and either pole. The relative difference between the semi-major and semi-minor axes (called the flattening) closes to 1/300. The gravity field potential is the sum of the potential of the Earth's gravitational attraction and the potential of the centrifugal force due to the Earth's rotation. The centrifugal force varies on latitude with a maximum at the equator and a minimum (zero) at both poles. The gravity (g), most important variable in geodesy, is generally 0.5% more at the poles than on the equator due to the flattening (less distance to the center of the Earth at the pole than on the equator) and the centrifugal force. Various global gravity field models have been developed to describe the three-dimensional Earth's gravity field potential, and in turn to identify the geoid undulation (N)[13]. However, the flattening of the Earth (1/300) and variation of g (0.5%) are neglected in oceanography.

The geostrophic and hydrostatic balances in the ocean are represented by

$$-(2\Omega \sin\varphi)v = -\frac{1}{\rho R cos\varphi}\frac{\partial p}{\partial \lambda}, \quad (2\Omega \sin\varphi)u = -\frac{1}{\rho R}\frac{\partial p}{\partial \varphi} \tag{1}$$

$$\frac{\partial p}{\partial z} = -\rho g_0 \tag{2}$$

where $g_0 = 9.81\,\mathrm{m/s^2}$, is the globally averaged gravity; (φ, λ, z) are the latitude, longitude, and vertical coordinate (positive upward); (u, v) are zonal and latitudinal components of the AGC; p is the pressure; $\Omega = 2\pi/(86400\,\mathrm{s})$, is the Earth rotation rate; and $R = 6.3781364 \times 10^7\,\mathrm{m}$, is the Earth radius. The equatorial zone (5°S–5°N) is not included in the analysis because the geostrophic balance (1) does not exist. Let the pressure field at N and S be represented by $p_N(\lambda, \varphi)$ and $p_S(\lambda, \varphi)$. Vertical integration of hydrostatic balance Eq. (2) from N to S gives the pressure at S

$$p_S(\lambda, \varphi) = p_N(\lambda, \varphi) - \int_{N(\lambda, \varphi)}^{S(\lambda, \varphi)} \rho(\lambda, \varphi, z) g_0 dz \tag{3}$$

Horizontal pressure gradients at S are given by

$$\frac{\partial p_S(\lambda, \varphi)}{\cos\varphi \partial\lambda} = \frac{\partial p_N(\lambda, \varphi)}{\cos\varphi \partial\lambda} - \left[\frac{\partial S(\lambda, \varphi)}{\cos\varphi \partial\lambda}\rho(\lambda, \varphi, S)g_0 - \frac{\partial N(\lambda, \varphi)}{\cos\varphi \partial\lambda}\rho(\lambda, \varphi, N)g_0\right] - \int_{N(\lambda,\varphi)}^{S(\lambda,\varphi)} g_0 \frac{\partial \rho(\lambda, \varphi, z)}{\cos\varphi \partial\lambda} dz, \tag{4a}$$

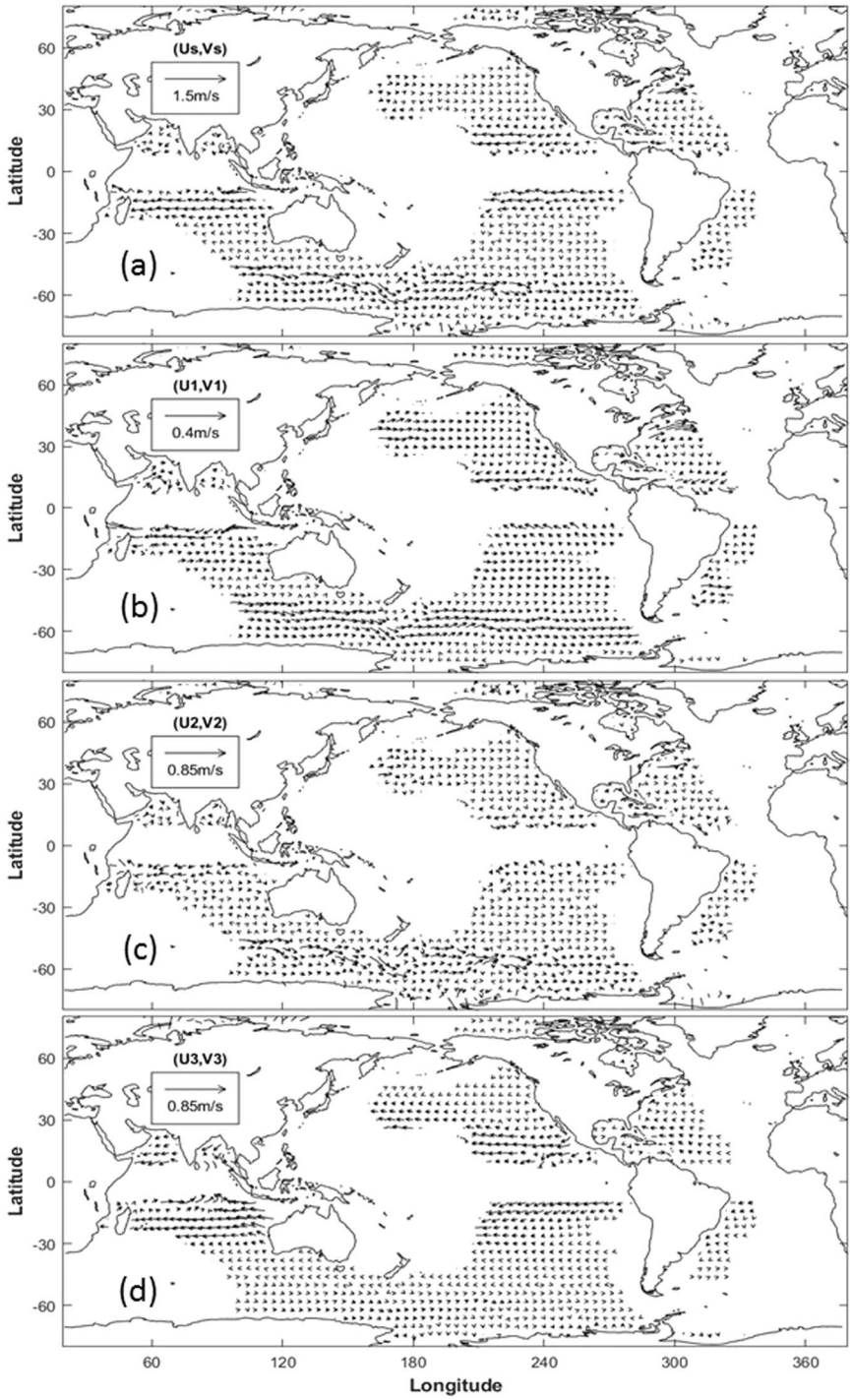

Figure 2. Velocity vectors for (**a**) AGC at the surface S, $\mathbf{v}_S$, (**b**) AGC at the geoid (N), $\mathbf{v}_1$, (**c**) geostrophic shear due to MDOT, $\mathbf{v}_2$, and (**d**) geostrophic shear due to density, $\mathbf{v}_3$. Note that areas in the equatorial (5°S to 5°N) and with $N > 0$ are not included. The total number of grid points are 15,481.

$$\frac{\partial p_S(\lambda,\varphi)}{\partial\varphi} = \frac{\partial p_N(\lambda,\varphi)}{\partial\varphi} - \left[\frac{\partial S(\lambda,\varphi)}{\partial\varphi}\rho(\lambda,\varphi,S)g_0 - \frac{\partial N(\lambda,\varphi)}{\partial\varphi}\rho(\lambda,\varphi,N)g_0\right] - \int_{N(\lambda,\varphi)}^{S(\lambda,\varphi)} g_0\frac{\partial\rho(\lambda,\varphi,z)}{\partial\varphi}dz \tag{4b}$$

The second terms in (4a and 4b) are re-written by

	Mean (cm/s)	Standard Deviation (cm/s)	Skewness	Kurtosis
$\mathbf{v}_S = (u_S, v_S)$	(2.72, 0.01)	(13.6, 7.51)	(−0.01, 0.51)	(4.10, 8.84)
$\mathbf{v}_1 = (u_1, v_1)$	(1.52, −0.09)	(4.24, 1.60)	(−0.70, 0.21)	(6.12, 4.96)
$\mathbf{v}_2 = (u_2, v_2)$*	(1.58, 0.12)	(8.44, 7.15)	(−0.21, −0.03)	(7.24, 7.55)
$\mathbf{v}_3 = (u_3, v_3)$	(−0.36, −0.04)	(1.36, 0.32)	(−3.72, −2.4)	(18.0, 14.50)

Table 1. Statistical characteristics of the AGC at the surface S ($\mathbf{v}_S$), AGC at the geoid undulation N ($\mathbf{v}_1$), geostrophic shear from N to S due to the horizontal gradient of the MDOT ($\mathbf{v}_2$), and due to the horizontal gradient of the density ($\mathbf{v}_3$), with the symbol '*' to represent the current practice in physical oceanography and satellite geodesy. Here, the statistical parameters were calculated from 15,481 data points of each velocity component.

$$-g_0\left[\frac{\partial S(\lambda,\,\varphi)}{\cos\varphi\partial\lambda}\rho(\lambda,\,\varphi,\,S) - \frac{\partial N(\lambda,\,\varphi)}{\cos\varphi\partial\lambda}\rho(\lambda,\,\varphi,\,N)\right] = -\rho_S g_0\left[\frac{\partial S(\lambda,\,\varphi)}{\cos\varphi\partial\lambda} - \frac{\rho_N}{\rho_S}\frac{\partial N(\lambda,\,\varphi)}{\cos\varphi\partial\lambda}\right] \tag{5a}$$

$$-g_0\left[\frac{\partial S(\lambda,\,\varphi)}{\partial\varphi}\rho(\lambda,\,\varphi,\,S) - \frac{\partial N(\lambda,\,\varphi)}{\partial\varphi}\rho(\lambda,\,\varphi,\,N)\right] = -\rho_S g_0\left[\frac{\partial S(\lambda,\,\varphi)}{\partial\varphi} - \frac{\rho_N}{\rho_S}\frac{\partial N(\lambda,\,\varphi)}{\partial\varphi}\right] \tag{5b}$$

Here, $\rho_S = \rho(\lambda,\,\varphi,\,S)$, $\rho_N = \rho(\lambda,\,\varphi,\,N)$, are the sea-water density at S and N. The density ratio $\rho_N/\rho_S \cong 1$ is due to the Boussinesq approximation. Substitution of (4a and 4b) into (1) leads to a complete formula for the surface AGC,

$$(u_S,\ v_S) = (u_1, v_1) + (u_2, v_2) + (u_3, v_3), \tag{6}$$

where (u_1, v_1) is the AGC at N;

$$u_2(\lambda,\,\varphi) = -\frac{g_0}{2\Omega\sin\varphi}\frac{\partial D(\lambda,\,\varphi)}{R\partial\varphi},\ \ v_2(\lambda,\,\varphi) = \frac{g_0}{2\Omega\sin\varphi}\frac{\partial D(\lambda,\,\varphi)}{R\cos\varphi\partial\lambda} \tag{7}$$

is the geostrophic shear from N to S due to horizontal gradient of D; and

$$\mathrm{u}_3(\lambda,\,\varphi) = -\frac{g_0}{2\Omega\sin\varphi}\int_{N(\lambda,\varphi)}^{S(\lambda,\varphi)}\frac{\partial\rho(\lambda,\,\varphi,\,z)}{R\partial\varphi}dz,\ \ \mathrm{v}_3(\lambda,\,\varphi) = \frac{g_0}{2\Omega\sin\varphi}\int_{N(\lambda,\varphi)}^{S(\lambda,\varphi)}\frac{\partial\rho(\lambda,\,\varphi,\,z)}{R\cos\varphi\partial\lambda}dz \tag{8}$$

is the geostrophic shear from N to S due to horizontal gradient of density. The formula (6) is not the mode decomposition of the surface AGC. It is just a horizontal differentiation of (3) with the righthand side containing the definite integral with variable upper limit $S(\lambda,\,\varphi)$ and lower limit $N(\lambda,\,\varphi)$, and shows the geostrophic shear from N to S containing the horizontal gradients of DOT ($\mathbf{v}_2$) and density ($\mathbf{v}_3$). The part of $\mathbf{v}_3$ is not included in $\mathbf{v}_2$.

Before satellites coming into practice, classical geodesy uses a theoretical hypothesis that the marine geoid is the ***average level of sea surface height if the water is at rest***, i.e., vanish of AGC at N, $(u_1, v_1) = 0$. After ignoring horizontal density gradient between S and N, $(u_3, v_3) = 0$, the AGC at the ocean surface is determined solely by the horizontal MDOT gradients,

$$u_S(\lambda,\,\varphi) = -\frac{g_0}{2\Omega\sin\varphi}\frac{\partial D(\lambda,\,\varphi)}{R\partial\varphi},\ \ v_S(\lambda,\,\varphi) = \frac{g_0}{2\Omega\sin\varphi}\frac{\partial D(\lambda,\,\varphi)}{R\cos\varphi\partial\lambda} \tag{9}$$

Similar idea [existence of a reference level of no motion (z_0)] prevails in oceanography for a long time in determination of AGC using hydrographic data, with various z_0 values (−500, −550, −650, −1000, −1200, −1800, −2000, −4000 m, …) by different people for different regions[14]. If the same formula (6) is used for the surface AGC [represented by $(\tilde{u},\,\tilde{v})$] with replacement of N by z_0, the AGC on z_0 is zero,

$$(\tilde{\mathrm{u}}_1,\ \tilde{\mathrm{v}}_1) = 0. \tag{10}$$

The second term in (6) becomes the horizontal gradient of sea surface height S since the reference level z_0 is flat,

$$\tilde{u}_2(\lambda,\,\varphi) = -\frac{g_0}{2\Omega\sin\varphi}\frac{\partial S(\lambda,\,\varphi)}{R\partial\varphi},\ \ \tilde{v}_2(\lambda,\,\varphi) = \frac{g_0}{2\Omega\sin\varphi}\frac{\partial S(\lambda,\,\varphi)}{R\cos\varphi\partial\lambda} \tag{11}$$

$$\tilde{\mathrm{u}}_3(\lambda,\,\varphi) = -\frac{g_0}{2\Omega\sin\varphi}\int_{z_0}^{S(\lambda,\varphi)}\frac{\partial\rho(\lambda,\,\varphi,\,z)}{R\partial\varphi}dz,\ \ \tilde{v}_3(\lambda,\,\varphi) = \frac{g_0}{2\Omega\sin\varphi}\int_{z_0}^{S(\lambda,\varphi)}\frac{\partial\rho(\lambda,\,\varphi,\,z)}{R\cos\varphi\partial\lambda}dz \tag{12}$$

Despite the uncertainty of z_0, Eqs. (10)–(12) are still used in oceanography such as ($z_0 = -1000$ m)[15] and ($z_0 = -500$ m)[16].

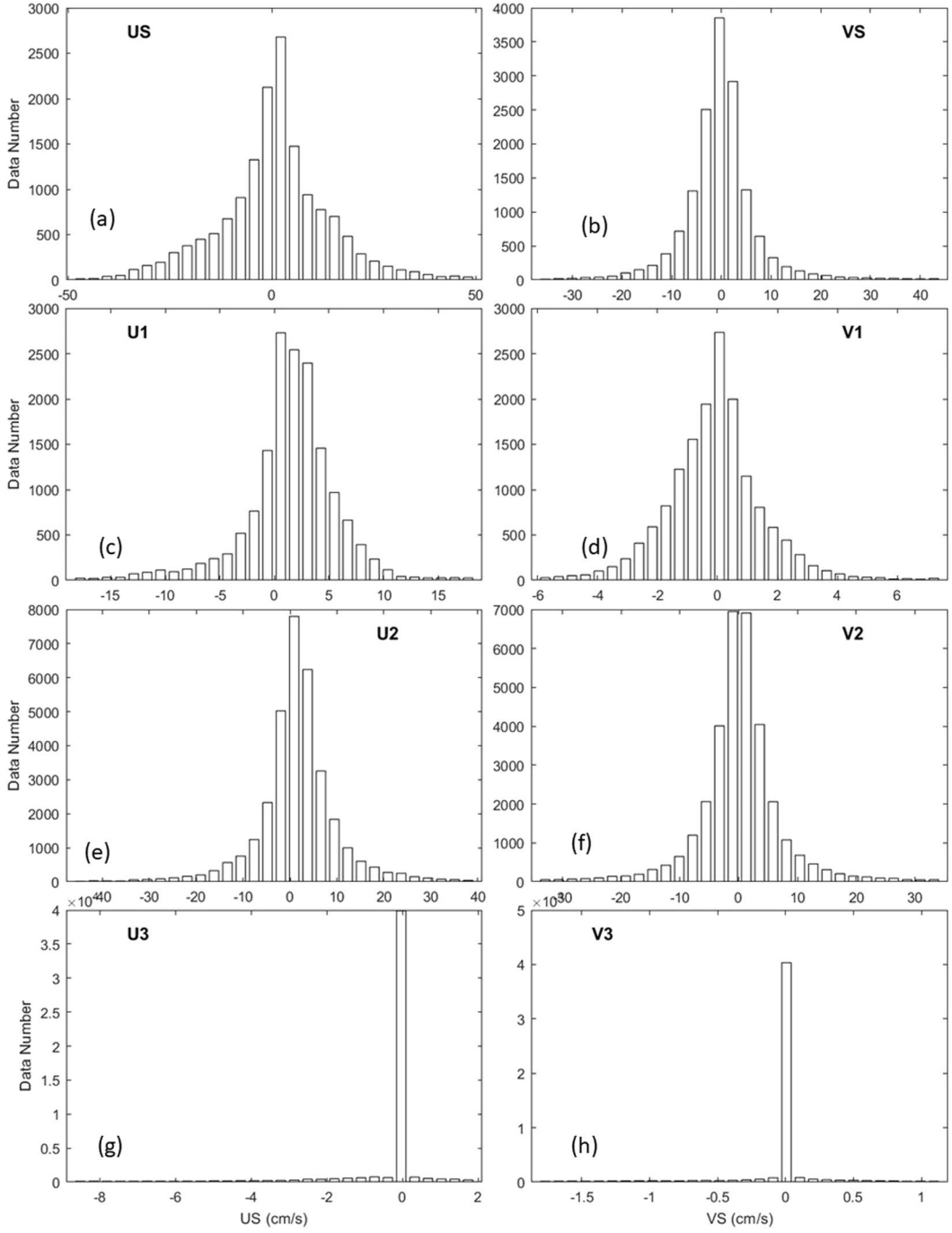

Figure 3. Histograms of (**a**) u_S, (**b**) v_S, (**c**) u_1, (**d**) v_1, (**e**) u_2, (**f**) v_2, (**g**) u_3, and (**h**) v_3. Evident difference of histograms between u_S and u_2 and v_S and v_2 indicates inaccuracy of using v_2 only to represent v_S (i.e., current practice in oceanography and satellite geodesy).

To eliminate the uncertainty in determining z_0, the geoid undulation N was suggested to replace z_0 as the reference level[17], i.e., use of (9) for the surface AGC. It becomes the common belief in marine geodesy and oceanography. Numerous papers have been published using the incomplete formula (9) to represent the surface AGC[18–24]. Note that the theoretical hypothesis of ***no motion at N*** hasn't been tested. Since satellite altimetry and gravimetry coming into practice, high-resolution observational sea surface height and gravity data were collected. The geoid undulation N was calculated by various gravity models. Now, it is ready to test this theoretical hypothesis (no motion at N) using existing three-dimensional climatological geostrophic current data. In addition, the error due to use of incomplete formula (9) can also be estimated.

Data sources. Four existing datasets were used in this study: (1) EIGEN-6C4 for N (http://dataservices.gfz-potsdam.de/icgem/showshort.php?id=escidoc:1119897)[13,25]; (2) world ocean geostrophic velocity inverted

Component of Surface AGC	Name of the Component	Relative Root Mean Square Difference between Component and $\mathbf{v}_S$
$\mathbf{v}_1 = (u_1, v_1)$	AGC at the Geoid N	0.866
$\mathbf{v}_2 = (u_2, v_2)$	Geostrophic Shear due to MDOT	0.605*
$\mathbf{v}_3 = (u_3, v_3)$	Geostrophic Shear due to Density	0.851
$\mathbf{v}_1 + \mathbf{v}_2$		0.540
$\mathbf{v}_S = \mathbf{v}_1 + \mathbf{v}_2 + \mathbf{v}_3$	Complete AGC at the Surface S	0

Table 2. Relative root mean square difference between each component and complete form of surface AGC with the symbol '*' to represent the current practice in physical oceanography and satellite geodesy.

from World Ocean Atlas 2013 (WOA13) with the P-Vector method (https://data.nodc.noaa.gov/cgi-bin/iso?id=gov.noaa.nodc:0121576) for the AGC at N, i.e., (u_1, v_1)[26,27]; (3) MDOT (https://grace.jpl.nasa.gov/data/get-data/dynamic-ocean-typography/) for calculating (u_2, v_2)[28], and (4) WOA13 temperature and salinity fields (https://www.nodc.noaa.gov/OC5/woa13/) for calculating (u_3, v_3).

EIGEN-6C4. EIGEN-6C4, elaborated jointly by GFZ Potsdam and GRGS Toulouse, is a static global combined gravity field model up to degree and order 2190. The model is on the website http://icgem.gfz-potsdam.de/home for public use[13,25]. The author ran the model with $1° \times 1°$ resolution for 17 seconds to get the global N (Fig. 1). ***Look at*** Fig. 1***, no one can claim no geostrophic currents on N***.

World ocean geostrophic velocity inverted from WOA13. This dataset comprises 3D gridded climatological fields of AGC inverted from World Ocean Atlas-2013 (WOA13) temperature and salinity fields using the P-vector method. It provides a climatological AGC field that is dynamically compatible to the WOA2013 (T, S) fields[26]. The dataset has the same spatial resolution and temporal variation (annual, monthly, seasonal) as WOA13 (T, S) fields, but does not cover the equatorial zone (5°S–5°N) due to the geostrophic balance being the theoretical basis for the P-vector inverse method[29]. This dataset can be downloaded from the NCEI website: https://data.nodc.noaa.gov/cgi-bin/iso?id=gov.noaa.nodc:0121576. This three-dimensional AGC dataset is in the z-coordinate system from z = 0 (top) to z = −8,900 m (bottom). Therefore, the AGC at N in the oceans can be obtained from this dataset with only non-positive N values. Positive N is out of the range of z [0 ≥ z ≥ −8,900 m], no data would be available from the climatological AGC field[26]. Altogether, we have 15,481 total data points. Figure 2b shows AGC vectors (u_1, v_1) at N.

MDOT. The MDOT data can be downloaded from NASA Jet Propulsion Laboratory web site: https://grace.jpl.nasa.gov/data/get-data/dynamic-ocean-typography/, with −1.9981 m as the minimum and 1.9538 m as the maximum. A tilt of S relative to N (i.e., MDOT) measures a part of the long-term averaged strength of geostrophic shear, (u_2, v_2) (Fig. 2c), rather than commonly thought AGC at the surface[6]. Also, water moves on S, how could the water not move on N (within 2 m above or below S)?

WOA13 temperature and salinity fields. The WOA13 climatological annual mean temperature and salinity fields with $1° \times 1°$ resolution were downloaded from the website https://www.nodc.noaa.gov/OC5/woa13/. The three-dimensional density $\rho(\lambda, \varphi, z)$ was calculated using the international thermodynamic equation of seawater-2010, which was downloaded from the website: http://unesdoc.unesco.org/images/0018/001881/188170e.pdf. Substitution of $\rho(\lambda, \varphi, z)$ into (8) leads to the long-term averaged geostrophic shear from N to S due to horizontal density gradient, (u_3, v_3) (Fig. 2d). If $S(\lambda, \varphi)$ takes positive values, the density between $z = S(\lambda,\varphi)$ and $z = 0$ take the value at z = 0. This is justifiable since the computation in this paper is limited for negative values of N, and the MDOT varies between −1.9981 m and 1.9538 m. The maximum positive value for $S(\lambda, \varphi)$ is less than 4 m, which is thinner than upper ocean mixed layer depth.

Statistical characteristics. Histograms of (u_S, v_S), (u_1, v_1), (u_2, v_2), and (u_3, v_3) (Fig. 3) and associated statistical parameters (Table 1) show evident difference between (u_S, v_S), and (u_2, v_2). Here, the statistical parameters (mean, standard deviation, skewness, and kurtosis) were calculated from 15,481 data points of each velocity component. All the velocity components have small mean values, small skewness for (u_S, v_S), (u_1, v_1), (u_2, v_2) (i.e., nearly symmetric) and large negative skewness (−3,72, −2.4) for (u_3, v_3). The standard deviation is much larger in u_S (13.60 cm/s) than in u_2 (8.44 cm/s), but comparable between v_S (7.51 cm/s) and v_2 (7.15 cm/s). This is due to small variabilities in v_1 (1.60 cm/s) and (0.32 cm/s). The kurtosis is much larger than 3 in all the components. The differences in the Kurtosis between u_S (4.10), and u_2 (7.24), and between v_S (8.84), and v_2 (7.55) are quite evident.

Relative root mean square difference. Summation of the three component vectors $\mathbf{v}_1 = (u_1, v_1)$, $\mathbf{v}_2 = (u_2, v_2)$, and $\mathbf{v}_3 = (u_3, v_3)$ gives ocean surface AGC vector $\mathbf{v}_S = (u_S, v_S)$. Figure 4 shows the relationships between each component $\mathbf{v}_K$ ($K = 1, 2, 3$) and as well as $\mathbf{v}_1 + \mathbf{v}_2$ versus $\mathbf{v}_S$. For each case, the relative root mean square difference (E) is computed by

$$E(\mathbf{v}_S, \mathbf{v}) = \sqrt{\sum_i \sum_j \left[(u_S - u)^2_{i,j} + (v_S - v)^2_{i,j}\right]} \Big/ \sqrt{\sum_i \sum_j \left[(u_S)^2_{i,j} + (v_S)^2_{i,j}\right]} \tag{13}$$

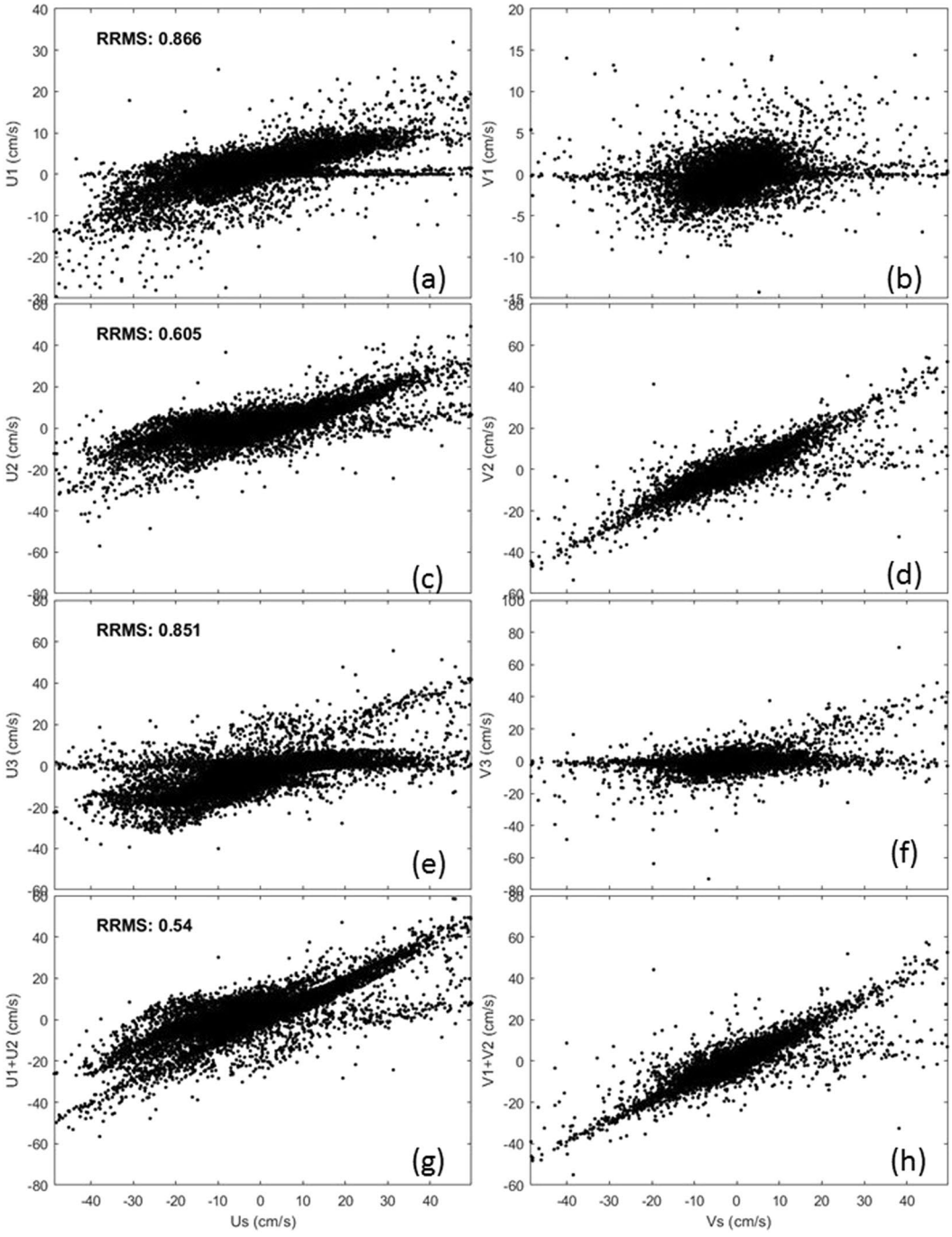

Figure 4. Scatter diagrams for (**a**) u_1 and u_S, (**b**) v_1 and v_S, (**c**) u_2 and u_S, (**d**) v_2 and v_S, (**e**) u_3 and u_S, (**f**) v_3 and v_S, (**g**) $(u_1 + u_2)$ and u_S, and (**h**) $(v_1 + v_2)$ and v_S. The relative root mean square difference between the component vectors and $\mathbf{v}_S$ are presented on the left panels.

where $\mathbf{v}$ is $\mathbf{v}_1$, $\mathbf{v}_2$, $\mathbf{v}_3$, or $\mathbf{v}_1 + \mathbf{v}_2$; (i, j) are the horizontal grid indices with the total grid points of 15,481. Table 2 lists the values of E for all the three components: 0.866, 0.605, and 0.851. It is noted that $\mathbf{v}_S$ is poorly correlated to $\mathbf{v}_1$, and $\mathbf{v}_3$, with large values of E (0.866, 0.851). This is due to large amount data of (u_1, v_1) and (u_3, v_3) near zero (also see Fig. 3c,d,g,h), with no connection to the change of (u_S, v_S). Dynamical mechanisms causing such poor correlations need to be explored further.

Evidence presented here shows that the relative root mean square difference between the surface AGC ($\mathbf{v}_S$) and the geostrophic shear due to horizontal gradient of MDOT ($\mathbf{v}_2$) is 0.605. Large differences in E and statistical parameters (mean, standard deviation, skewness, and kurtosis) show that the current practice in physical oceanography and satellite geodesy (representing $\mathbf{v}_S$ by $\mathbf{v}_2$) is questionable. It is important to add the absolute geostrophic current at the geoid ($\mathbf{v}_1$) and the geostrophic shear due to inhomogeneous density ($\mathbf{v}_3$).

Received: 8 September 2019; Accepted: 10 January 2020;
Published online: 29 January 2020

References

1. Fu, L. L. & Haines, B. J. The challenges in long-term altimetry calibration for addressing the problem of global sea level change. *Adv. Space Res.* **51**, 1284–1300 (2013).
2. Shum, C. *et al.* Calibration of JASON-1 Altimeter over Lake Erie Special Issue: Jason-1 Calibration/Validation. *Mar. Geod.* **26**, 335–354 (2003).
3. Johannessen, J. A. *et al.* The European Gravity Field and Steady-State Ocean Circulation Explorer satellite mission its impact on geophysics. *Surv. Geophys.* **24**, 339–386 (2003).
4. Jet Propulsion Laboratory. *Gravity Recovery and Climate Experiment (GRACE)*. Science and mission requirements document, revision A, JPLD-15928, NASA's Earth Syst. Sci. Pathfinder Program, 1–84 (1998).
5. Bruinsma *et al*. The new ESA satellite-only gravity field model via the direct approach. *Geophys. Res. Lett* **40**, 3607–3612 (2013).
6. Chu, P. C. Two types of absolute dynamic ocean topography. *Ocean Sci.* **14**, 947–957 (2018).
7. Stommel, H. & Schott, F. The beta spiral and the determination of the absolute velocity field from hydrographic station data. *Deep Sea Res.* **24**, 325–329 (1977).
8. Wunsch, C. The general circulation of the North Atlantic west of 50° W determined from inverse methods. *Rev. Geophys.* **16**, 583–620 (1978).
9. Chu, P. C. P-vector method for determining absolute velocity from hydrographic data. *Mar. Tech. Soc. J.* **29**(3), 3–14 (1995).
10. Chu, P. C., Fan, C. W., Lozano, C. J. & Kerling, J. An AXBT survey of the South China Sea. *J. Geophy. Res.* **103**, 21637–21652 (1998).
11. Chu, P. C. & Li, R. F. South China Sea isopycnal surface circulations. *J. Phys. Oceanogr.* **30**, 2419–2438 (2000).
12. Yuan, D. L., Zhang, Z. C., Chu, P. C. & Dewar, W. K. Geostrophic circulation in the tropical north Pacific Ocean based on Argo profiles. *J. Phys. Oceanogr.* **44**, 558–574 (2014).
13. Ince, E. S. *et al.* ICGEM – 15 years of successful collection and distribution of global gravitational models, associated services, and future plans. *Earth Syst. Sci. Data* **11**, 647–674 (2019).
14. Defant, A. *Physical Oceanography*, Vol 1, 492–494 (Pergamon Press, 1961).
15. Osiński, R., Wieczorek, P., Beszczyńska-Möller & Goszczko, I. ADCP-referenced geostrophic velocity and transport in the West Spitsbergen. *Current. Oceanol.* **45**, 425–435 (2003).
16. Tagi, A. M., Al-Subhi, A. M., Alsaafani, M. A. & Abdulla, C. P. Estimation of geostrophic current in the Red Sea based on sea level anomalies derived from extended satellite altimetry data. *Ocean Sci.* **15**, 477–488 (2019).
17. Wunsch, C. & Gaposchkin, E.-M. On using satellite altimetry to determine the general circulation of the ocean with application to geoid improvement. *Rev. Geophys.* **18**, 725–745 (1980).
18. Tapley, B. D., Chambers, D. P., Bettadpur, S. & Ries, J. C. Large scale ocean circulation from the GRACE GGM01 geoid. *Geophys. Res. Lett.* **30**, 2163, https://doi.org/10.1029/2003GL018622 (2003).
19. Knudsen, P., Bingham, R., Andersen, O. & Rio, M.-H. A global mean dynamic topography and ocean circulation estimation using a preliminary GOCE gravity model. *J. Geod.* **85**, 861–879 (2011).
20. Sánchez-Reales, J. M., Vigo, M. I., Jin, S. & Chao, B. F. Global surface geostrophic ocean currents derived from satellite altimetry and GOCE geoid. *Mar. Geod.* **35**, 175–189 (2012).
21. Sudre, J., Maes, C. & Garçon, V. On the global estimates of geostrophic Ekman surface currents. *Limn. Oceanogr. Fluids & Environ.* **3**, 1–20 (2013).
22. Jin, S., Feng, G. & Andersen, O. Errors of mean dymanic topography and geostrophic current estimates in China's marginal seas from GOCE and satellite altimetr. *y. J. Atmos. Oceanic Technol.* **31**, 2544–2555 (2014).
23. Rio, M.-H., Mulet, S. & Picot, N. Beyond GOCE for the ocean circulation estimate: Synergetic use of altimetry, gravimetry, and *in situ* data provides new insight into geostrophic and Ekman currents. *Geophys. Res. Lett.* **41**, 8918–8925 (2014).
24. Chang, C.-H., Kuo, C.-Y., Shum, C. K., Yi, Y. & Rateb, A. Global surface and subsurface geostrophic currents from multi-mission satellite altimetry and hydrographic data, 1996–2011. *J. Mar. Sci. Technol.* **24**, 1181–1193 (2016).
25. Förste, C. *et al.*. *EIGEN-6C4*. The latest combined global gravity field model including GOCE data up to degree and order 2190 of GFZ Potsdam and GRGS Toulouse. GFZ Data Services. https://doi.org/10.5880/icgem.2015.1 (2014).
26. Chu, P. C. & Fan, C. W. Absolute geostrophic velocity inverted from World Ocean Atlas 2013 (WOAV13) with the P-vector method. *Geosci. Data J.* **2**, 78–82 (2015).
27. Chu, P. C. World ocean isopycnal level absolute geostrophic velocity inverted from GDEM with the P-Vector method. *MDPI Data* **3**, 1, https://doi.org/10.3390/data3010001 (2018).
28. Pavlis, N. K., Holmes, S. A., Kenyon, S. C. & Factor, J. K. The development and evaluation of the Earth Gravitational Model 2008 (EGM2008). *J. Geophys. Res.* **117**, B04406 (2012).
29. Chu, P. C. *P-Vector Inverse Method*, 1–605 (Springer Press, 2006).

Acknowledgements

The author thanks the International Centre for Global Erath Models (ICGEM) for the EIGEN-6C4 geoid undulation data, the NASA Jet Propulsion Laboratory (JPL) for the mean dynamic ocean topography data, and the NOAA National Centers for Environmental Information (NCEI) for the World Ocean Atlas 2013 temperature and salinity fields and corresponding absolute geostrophic velocity inverted by the P vector method. He also thanks Mr. Chenwu Fan for computational assistance.

Author contributions

P.C.C. derived the complete formula for the ocean surface absolute geostrophic current, designed the project, obtained the datasets, conducted the computation, and wrote the manuscript.

Competing interests

The author declares no competing interests.

Additional information

Supplementary information is available for this paper at https://doi.org/10.1038/s41598-020-58458-w.

Correspondence and requests for materials should be addressed to P.C.C.

Reprints and permissions information is available at www.nature.com/reprints.